Constraining black hole mimickers with gravitational wave observations

Nathan K. Johnson-McDaniel,[1,2] Arunava Mukherjee,[1,3,4] Rahul Kashyap,[1]
Parameswaran Ajith,[1,5] Walter Del Pozzo,[6,7,8] and Salvatore Vitale[9]

[1]*International Centre for Theoretical Sciences, Tata Institute of Fundamental Research, Bengaluru 560089, India*
[2]*Department of Applied Mathematics and Theoretical Physics, Centre for Mathematical Sciences, University of Cambridge, Cambridge, CB3 0WA, United Kingdom*
[3]*Albert-Einstein-Institut, Max-Planck-Institut für Gravitationsphysik, Callinstr. 38, D-30167 Hannover, Germany*
[4]*Leibniz Universität Hannover, D-30167 Hannover, Germany*
[5]*Canadian Institute for Advanced Research, CIFAR Azrieli Global Scholar, MaRS Centre, West Tower, 661 University Ave., Suite 505, Toronto, ON M5G 1M1, Canada*
[6]*School of Physics and Astronomy, University of Birmingham, Edgbaston, Birmingham, B15 2TT, United Kingdom*
[7]*Universitá di Pisa, I-56127 Pisa, Italy*
[8]*INFN, Sezione di Pisa, I-56127 Pisa, Italy*
[9]*LIGO Laboratory and Kavli Institute for Astrophysics and Space Research, Massachusetts Institute of Technology, Cambridge, Massachusetts 02139, USA*

LIGO and Virgo have recently observed a number of gravitational wave (GW) signals that are fully consistent with being emitted by binary black holes described by general relativity. However, there are theoretical proposals of exotic objects that can be massive and compact enough to be easily confused with black holes. Nevertheless, these objects differ from black holes in having nonzero tidal deformabilities, which can allow one to distinguish binaries containing such objects from binary black holes using GW observations. Using full Bayesian parameter estimation, we investigate the possibility of constraining the parameter space of such "black hole mimickers" with upcoming GW observations. Employing perfect fluid stars with a polytropic equation of state as a simple model that can encompass a variety of possible black hole mimickers, we show how the observed masses and tidal deformabilities of a binary constrain the equation of state. We also show how such constraints can be used to rule out some simple models of boson stars.

Introduction:— The Advanced LIGO [1] and Advanced Virgo [2] detectors have recently observed several gravitational-wave (GW) signals from the coalescences of compact binaries [3–9]. The measured component masses and general characteristics of chirping signals in these events establish that the component objects in these binaries are extremely compact and massive, strongly suggesting that they are stellar-mass black holes [3–8] or neutron stars [9]. In addition, for the putative binary black hole events, the data are found to be fully consistent with binary black hole solutions in general relativity, as established by several consistency tests [4–8, 10].

However, there are theoretical proposals of exotic alternatives to black holes, which can be massive and compact enough so that GWs from binaries of such objects can be confused with those from binary black holes, e.g., [11–15]. One commonly considered alternative to black holes are boson stars [16] – gravitational equilibrium configurations of a massive, possibly self-interacting, scalar field; the axion is one possibility for such a field. Other alternatives include dark matter stars made of bosonic or fermionic particles (see, e.g., [11]). If the masses of these particles are sufficiently small or their self-interactions are sufficiently strong, they can form stars that are massive and compact enough to explain at least the general properties of the GW signals currently identified as coming from binary black hole coalescences. Other examples include gravastars – hypothetical objects with a de Sitter space interior surrounded by a shell of matter [17].

Potential electromagnetic or astroparticle (e.g., neutrino) signatures of the coalescences of binaries containing such exotic objects are not well understood. Additionally, even in the case of scalar field stars (including boson stars), which is the most straightforward to model numerically, simulations of the coalescences of such binaries are still in the exploratory phase, e.g., [13, 18–21]. However, there are robust features that distinguish gravitational waveforms of binaries containing material objects from those of binary black holes. In particular, material objects will be deformed by the tidal field of their companion as well as by their own spin, and these deformations will affect the objects' gravitational fields, and thus the binary's gravitational waveform (from changes to its binding energy and radiative multipole moments, in the post-Newtonian picture). Post-Newtonian (PN) calculations of the effects of such changes to the multipole moments of the components of the binary are well-developed and can be used to model the inspiral waveforms of binaries of black hole mimickers, allowing one to distinguish binaries of such objects from binary black holes. The idea of constraining properties of specific black hole mimickers using constraints on the tidal deformabilities has been proposed in [14, 22] (with initial work on constraining the tidal deformability of black holes in [23] and general theoretical proposals for such tests in [24]), while [25] consider using the spin-induced quadrupole moment and [26] consider using the differences in tidal heating. Note that all of the data analysis studies to date use the Fisher matrix approximation [27].

In this Letter, we present a Bayesian method for distinguishing such exotic compact objects from binary black hole mergers based on the measurement of the tidal deformability. Alternatively, a null measurement will place an upper limit on the tidal deformability and hence will constrain the parameter space of various black-hole mimickers. This is the first full statistical analysis of this problem, without using the Fisher matrix approximation, and makes use of some of the best available gravitational waveforms. Additionally, it self-consistently takes into account the fact that black hole mimickers can merge at significantly lower frequencies than their black hole counterparts, both due to their larger radius and due to the tidal deformation that we aim to constrain. We use perfect fluid stars with a polytropic equation of state as a simple model that

can encompass a variety of black hole mimickers.

A simple model for black hole mimickers:— For this initial study, we consider nonspinning, perfect fluid stars described by a polytropic equation of state (EOS). The matter in the star is thus described by an energy density ϵ and pressure p, related by $p = K\rho^{1+1/n}$, where $K > 0$ and $n > 0$ are the polytropic constant and index, respectively, and $\rho = \epsilon - n\,p$ is the rest mass density. While this is a very simple model, polytropic EOSs nevertheless provide a good description of the structure of some potential black hole mimickers, as shown in [11]. We also show in the Supplemental Material that the tidal deformability-mass relationships for more compact boson stars (from [14, 28]) are well approximated (at least in the quadrupolar and octupolar cases) by those of stars with polytropic EOSs.

Properties of these stellar models that are relevant for this investigation are their radii and multipolar tidal deformabilities for a given mass. These quantities determine the contact frequency, as well as the effects of the objects' tidal interactions on the waveform. We only need the dominant quadrupolar tidal deformability to model the waveforms to the accuracy necessary for the present study, but require higher multipolar tidal deformabilities to accurately model the contact frequency. We compute the stellar structure and tidal deformabilities in the standard way, by solving the Oppenheimer–Volkov equations for the stellar structure and then using the expressions from [29] to obtain the tidal deformabilities. The final output is the radii and tidal deformabilities as a function of mass up to the maximum mass allowed by the EOS.

Specifically, we consider the dimensionless quadrupolar tidal deformability $\Lambda := \lambda/M^5$, where λ is the dimensionful quadrupolar tidal deformability and M is the star's mass [30]. Here λ is given by $Q_{ij} = -\lambda\,\mathcal{E}_{ij}$, where Q_{ij} is the star's induced quadrupole moment and $\mathcal{E}_{ij}$ is the external tidal field (see, e.g., [31]), all measured in mass units. The minimum value of Λ (for a stable star), $\Lambda_{\rm min}$, is attained by the maximum mass ($M_{\rm max}$) stable star, and since Λ is dimensionless, $\Lambda_{\rm min}$ only depends on n, not K. The $\Lambda_{\rm min}$ values for the polytropic indices we consider range from 3.7 for $n = 0.5$ to 8500 for $n = 2$, and the associated minimum radii are 1.58 to 6.75 times the Schwarzschild radius associated with the star's mass.

Inspiral waveforms for black hole mimickers:— During the early stages of their inspiral, the compact objects can be approximated as point particles endowed with a tidally-induced quadrupole moment and their dynamics and gravitational waveforms can be computed in the PN approximation to general relativity, where one expands in terms of a small velocity parameter v in units of c [32]. The PN waveforms describing binaries of nonspinning point particles are currently known up to $O(v^7)$ beyond the leading order. Tidal effects first appear in the waveform as a high order $O(v^{10})$ correction, but they can still have an appreciable effect on the waveforms depending on the value of the tidal deformability Λ.

The PN description of the point-particle portion of the waveform is not sufficiently accurate to describe the late inspiral where tidal effects are the largest (see, e.g., [33]). Thus, in the absence of accurate numerical simulations of binaries of black hole mimickers, we model the waveforms of these binaries of polytropic stars using the frequency-domain binary black hole waveform model IMRPhenomD [34], to give a model for the point-particle part of the waveform that is more accurate in the late inspiral than pure PN results. In particular, IMRPhenomD contains effective $O(v^8)$ though $O(v^{10})$ terms in the inspiral phasing that are calibrated to numerical relativity simulations of binary black holes. To model the tidal effects, we add tidal corrections accurate to $O(v^{12})$ computed in the stationary phase approximation [30, 35] to these waveforms' phase, similar to [36].[1] We have checked that the dephasing due to the partially known higher order tidal terms and differences in tidal heating [38–42] that we neglect here are small and/or do not improve agreement with numerical simulations of binary neutron stars [43]. Details are given in the Supplemental Material.

m_1^z, m_2^z $[M_\odot]$	d_L [Mpc]	SNR in O3 ("late-high" PSD)
39.5, 31.7	397.7	43.5
36.8, 22.9	592.4	24.7
27.6, 15.6	620.6	18.2
15.5, 8.2	292.5	24.4

TABLE I: Detector frame (i.e., redshifted) masses and luminosity distance of simulated binary black-hole events, replicating the first four GW signals observed by the LIGO detectors [3–6]. We give the SNRs of the injections in Advanced LIGO's "late-high" PSD [50] (comparable to the expected sensitivity in the third observing run O3).

Since our waveform models include the effects of tidal deformations using linear adiabatic tides, they are only accurate when the stars are sufficiently well-separated and not too tidally deformed. In particular, the models will definitely be inaccurate once the two stars have come into contact. We thus need to estimate the frequency at which a binary with given masses and tidal deformabilities will come into contact or have a tidal deformation greater than a given amount. Here we measure the tidal deformability using the star's fractional surface deformation, and take a maximum allowed value to be 0.2, at which point we assume that linear tidal deformations are no longer an accurate description of the system.

We estimate the contact frequency by extending the implicit expression for the contact separation given for binary neutron stars in [44]. This expression includes the leading effects of tidal deformability on the contact separation using the stars' quadrupolar shape tidal deformabilities [29, 45]. We extend this expression to include higher multipoles and higher PN corrections to the tidal fields, from [46]. We then compute the frequency from the contact separation using a PN expression. When we apply this expression to binary neutron stars, we find good agreement with numerical relativity results for polytropic stars from the literature [47–49]. Details are given in the Supplemental Material. Note that in the following, for brevity, we will use the term "contact frequency" to refer to the minimum of this contact frequency and the frequency at which one of the objects first has a surface deformation of 0.2.

Constraining the properties of polytropic stars with GW observations:— GW signals from the quasi-circular inspiral

[1] Since we add the tidal corrections to binary black hole waveforms, it is consistent for us to take the tidal Love number of a black hole to be zero, even with the ambiguity in the mapping from the standard calculations of Love numbers to the tidal terms in the waveform discussed by Gralla [37].

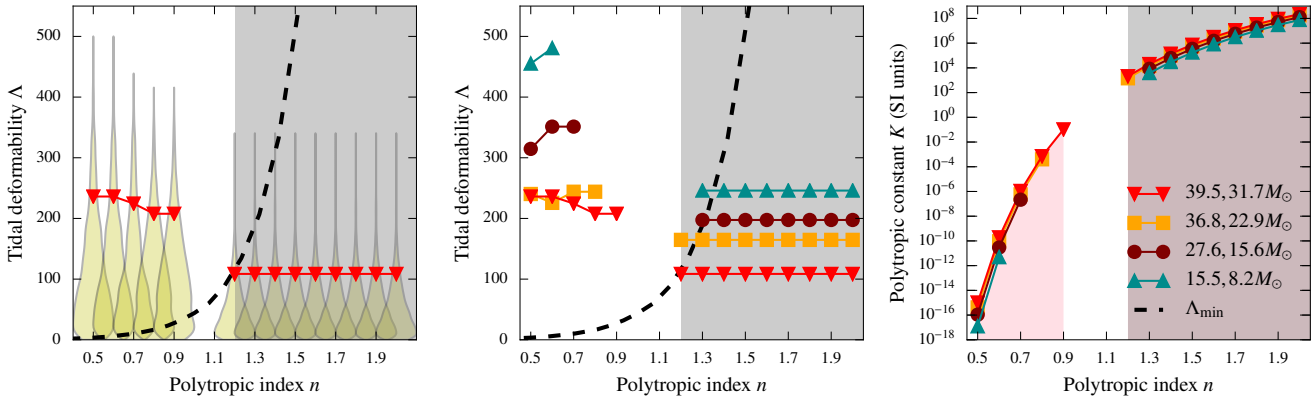

FIG. 1: *Left panel:* The dashed line shows the minimum value $\Lambda_{\rm min}$ of the dimensionless tidal deformability parameter allowed by the polytropic EOS, plotted against the polytropic index n. The violin plots show the marginalized posterior distribution of Λ_1 from a simulated event with (detector frame) masses of 39.5 and 31.7$M_\odot$ while the red triangles show the 90% credible upper bounds $\Lambda_{\rm UL}$. The shaded region shows the values of n for which the observed upper bounds $\Lambda_{\rm UL}$ are lower than the theoretical minimum $\Lambda_{\rm min}$ for the EOS, and hence can be ruled out. In all panels, the values of n for which there are no points for a given event are those values for which there are not a sufficient number of posterior samples satisfying the selection criteria discussed in the text (i.e., contact frequency > cutoff frequency used in the parameter estimation or $\Lambda_1 < \Lambda_{\rm min}$). *Middle panel:* Same as the left panel, except that we show the upper bounds obtained from all four simulated events (masses shown in legend). We show the largest exclusion region, corresponding to the most massive system considered (the same one as in the left panel). *Right panel:* The maximum value of the polytropic constant K (for a given polytropic index n) that is unconstrained by the observed lower limit $m_{\rm LL}$ on the mass of the compact object for all four simulated events. The pink shaded region is the largest region excluded by such an observation, and corresponds to the most massive system considered (the same one as in the left panel). The gray shaded region corresponds to the $\Lambda_{\rm min}$ constraint from the same system.

of nonspinning compact binaries are characterized by the set of intrinsic parameters $\{m_1, m_2, \Lambda_1, \Lambda_2\}$ (as well as higher-order tidal deformability and tidal heating coefficients that are negligible at the accuracies to which we are working) and several extrinsic parameters describing the location, orientation and the arrival time of the signals at the detector. We simulate observations of nonspinning binary black holes with parameters similar to LIGO's first four putative binary black hole events, using the median values of the masses in the detector frame (i.e., including cosmological redshift) [3–6].[2]

The sky-location and orientation of the binaries were chosen in such a way that the signal-to-noise ratio (SNR) of the signals is consistent with the expected distributions in the upcoming observations (see Table I). We then estimate the posterior distributions of these parameters using the LALInferenceNest code [51], which provides an implementation of the Nested Sampling algorithm [52] in the LALInference software [53]. We use flat priors on $m_1, m_2, \Lambda_1, \Lambda_2$; for derived quantities we use the priors induced from these flat priors. We have checked that the data are sufficiently informative that the posteriors do not resemble the priors. The parameter estimation is performed assuming a two-detector Advanced LIGO network with sensitivity anticipated in the upcoming observational run [modeled by the "late-high" power spectral density (PSD) [50] with a low-frequency cutoff of 15 Hz]. We choose to present the expected results from future observations since the SNRs available for the existing events do not allow us to derive interesting constraints using the self-consistent analysis that we describe below.

Note that, depending on the EOS, the compact objects can come in contact at different GW frequencies, causing the inspiral to end. Thus, for each simulated observation, we compute the posterior distributions by truncating the likelihood integral at different cutoff frequencies, and compute the 90% credible upper limits on Λ_1, Λ_2 and lower limits on m_1, m_2 from the marginalized one-dimensional posteriors. When constraining the EOS, for each value of the polytropic index n, we choose the upper/lower limits derived using an appropriate choice of the cutoff frequency (see below).

We compute the contact frequency assuming that both stars have the same polytropic index n, but possibly different polytropic constants K. We then choose the largest cutoff frequency such that 90% of the posterior samples that have both Λs above the minimum allowed by the EOS correspond to a contact frequency greater than the cutoff frequency employed in the posterior computation.[3] If the best 90% credible upper bound $\Lambda_{\rm UL}$ on the tidal deformability is smaller than the $\Lambda_{\rm min}$ corresponding to this EOS, the data exclude the possibility of both stars being described by this EOS at high confidence. Moreover, for a given polytropic index n, the minimum $M_{\rm max}$ sets the minimum allowed value of the polytropic constant K. Therefore, the best 90% credible lower bound $m_{\rm LL}$ on the component masses puts a constraint on K for the values of n

[2] Note that all the LIGO-Virgo events that we simulate, except the lowest-mass one, are consistent with binaries of *nonspinning* objects at the 90% credible level [3–6].

[3] We allow the stars to have different polytropic constants since we do not expect the structure of black hole mimickers to be described exactly by a polytropic equation of state. We could also allow the stars to have different polytropic indices, but for simplicity have not allowed that extra freedom in this initial study.

that are not ruled out by the tidal deformability constraint. We give more details in the Supplemental Material.

Figure 1 (left and middle panels) shows the estimated $\Lambda_{\rm UL}$ for various polytropic indices. The shaded region corresponds to observed $\Lambda_{\rm UL} < \Lambda_{\rm min}$ (theoretical), and is therefore ruled out by such a GW event. In the right panel, in addition to the excluded region in n from the tidal deformation, we also show the shaded region in $n - K$ space that is ruled out by having the observed $m_{\rm LL} > M_{\rm max}$. Details about the constraints on the radii of the stars, their closeness to the maximum mass of the EOS, and the cutoff frequencies used (including a comparison to binary black hole merger frequencies [54]) are given in the Supplemental Material.

Constraints on boson star models:— Here we show how the constraints on the maximum mass and minimum tidal deformability of black hole mimickers obtained in our general polytropic star framework can be translated into constraints on boson star models. This is only a proof of principle, because boson stars are not exactly described by a polytropic EOS, so the frequency cutoffs used to obtain these constraints are not exactly the ones one would obtain in applying the same procedure to more realistic boson star models. However, we find that the tidal deformability versus mass curves of compact boson stars are well approximated by those of polytropic stars, so these results are likely close to those that would be obtained in a fully consistent analysis.

As discussed earlier, boson stars are equilibrium configurations of a massive, complex scalar field ϕ. We consider boson stars with a boson mass m_B and a quartic self-interaction given by a potential $V(|\phi|^2) = m_B^2|\phi|^2 + \lambda_B|\phi|^4/2$, where λ_B is the coupling constant of the quartic self-interaction term. Such stars were first considered in [55], and their tidal deformabilities are calculated in [14, 22]. One can produce the observed masses of the objects in the binary for sufficiently small boson masses even in the *free-field* case ($\lambda_B = 0$). Specifically, one needs $m_B \lesssim (10^{-10}\ {\rm eV})(M_\odot/M_{\rm max})$; see, e.g., [22]. Increasing the self-interaction increases the allowed boson mass. However, for the quartic potential, $\Lambda > 287$, regardless of the strength of the coupling [56]. Thus, the tidal deformability constraints presented in Fig. 1 rule out a binary of quartic-potential boson stars as the source for these signals at the 90% credible level, except for the low-n results for the least massive case. However, low-n polytropic stars (with $n \lesssim 1.4$) have minimum tidal deformabilities smaller than the minimum allowed for quartic potential boson stars, and thus should not be considered for this analysis. Thus, binaries of quartic-potential boson stars (and also free-field boson stars) are ruled out at the 90% credible level as potential sources for all four simulated events. If one has less stringent upper bounds on tidal deformability, these bounds can be used to constrain the allowed (m_B, λ_B) parameter space; see the Supplemental Material.

Summary and outlook:— We have introduced a Bayesian method for constraining the properties of black hole mimickers such as boson stars or gravastars using GW observations. These constraints come from assuming that both members of the binary that created the GWs belong to the same family of black hole mimickers, so that the measured masses and tidal deformabilities give a lower limit on the maximum mass and upper bound on the minimum tidal deformability allowed for this family. In the absence of accurate numerical calculations of waveforms from binaries of black hole mimickers, we model them as perfect fluid stars with a polytropic EOS. We have presented sample constraints on polytropic parameters using simulated observations of binary black holes with parameters similar to the first four binary black hole events observed by Advanced LIGO. Additionally, as a proof of principle, we have shown that these constraints rule out binaries of boson stars constructed using either a noninteracting scalar field or a quartically interacting scalar field model as sources of the modelled GW signals.

Our present work does not consider spin, which would introduce a number of complications, due to the presence of spin-induced deformations [57] as well as spin-tidal couplings, which are just beginning to be explored (e.g., [58–61]). Improving the waveform models to include the spinning case will be the subject of future work. Ultimately, one needs numerical simulations of binaries of black hole mimickers with which to test current waveform models and calibrate new ones. Additionally, our use of polytropic stars excludes cases where the tidal deformability is negative, e.g., most gravastar models [62, 63]. We plan to consider gravastar models in future work. As theoretical studies mature, and the sensitivity of advanced GW detectors increases, we are presented with a real possibility of significantly constraining theoretical models of exotic compact objects, or detecting such objects in nature.

Acknowledgments:— We thank Tim Dietrich, Tanja Hinderer, Philippe Landry, Eric Poisson, and Rafael Porto for useful comments and discussion, Noah Sennett for providing clarifications about his work and producing the fit for the minimum tidal deformability, and Aaron Zimmerman for a careful reading of the manuscript. N. K. J.-M. acknowledges support from the AIRBUS Group Corporate Foundation through a chair in "Mathematics of Complex Systems" at the International Centre for Theoretical Sciences (ICTS) and from STFC Consolidator Grant No. ST/L000636/1. Also, this work has received funding from the European Union's Horizon 2020 research and innovation programme under the Marie Skłodowska-Curie grant agreement No. 690904. A. M. acknowledges support by a "Start-up grant for Young Scientists" (SB/FTP/PS-067/2014) by the Science and Engineering Research Board (SERB), India. P. A.'s research was supported by a Ramanujan Fellowship from the SERB, by the Max Planck Society through a Max Planck Partner Group at ICTS and by the Indo-US Centre for the Exploration of Extreme Gravity funded by the Indo-US Science and Technology Forum (IUSSTF/JC-029/2016). LIGO was constructed by the California Institute of Technology and Massachusetts Institute of Technology with funding from the National Science Foundation and operates under cooperative agreement PHY-0757058. Computations were performed at the ICTS cluster Alice. This is LIGO document P1800092.

[1] J. Aasi et al. (LIGO Scientific Collaboration), Classical Quantum Gravity **32**, 074001 (2015), 1411.4547.
[2] F. Acernese et al. (Virgo Collaboration), Classical Quantum Gravity **32**, 024001 (2015), 1408.3978.
[3] B. P. Abbott et al. (LIGO Scientific Collaboration and Virgo Collaboration), Phys. Rev. Lett. **116**, 061102 (2016), 1602.03837.
[4] B. P. Abbott et al. (LIGO Scientific Collaboration and Virgo Col-

laboration), Phys. Rev. Lett. **116**, 241103 (2016), 1606.04855.
[5] B. P. Abbott et al. (LIGO Scientific Collaboration and Virgo Collaboration), Phys. Rev. X **6**, 041015 (2016), 1606.04856.
[6] B. P. Abbott et al. (LIGO Scientific Collaboration and Virgo Collaboration), Phys. Rev. Lett. **118**, 221101 (2017).
[7] B. P. Abbott et al. (LIGO Scientific Collaboration and Virgo Collaboration), Phys. Rev. Lett. **119**, 141101 (2017), 1709.09660.
[8] B. P. Abbott et al. (LIGO Scientific Collaboration and Virgo Collaboration), Astrophys. J. Lett. **851**, L35 (2017), 1711.05578.
[9] B. P. Abbott et al. (LIGO Scientific Collaboration and Virgo Collaboration), Phys. Rev. Lett. **119**, 161101 (2017), 1710.05832.
[10] B. P. Abbott et al. (LIGO Scientific Collaboration and Virgo Collaboration), Phys. Rev. Lett. **116**, 221101 (2016), 1602.03841.
[11] G. F. Giudice, M. McCullough, and A. Urbano, J. Cosmol. Astropart. Phys. **1610**, 001 (2016), 1605.01209.
[12] R. F. P. Mendes and H. Yang, Classical Quantum Gravity **34**, 185001 (2017), 1606.03035.
[13] V. Cardoso, S. Hopper, C. F. B. Macedo, C. Palenzuela, and P. Pani, Phys. Rev. D **94**, 084031 (2016), 1608.08637.
[14] V. Cardoso, E. Franzin, A. Maselli, P. Pani, and G. Raposo, Phys. Rev. D **95**, 084014 (2017), 1701.01116.
[15] V. Cardoso and P. Pani, Nat. Astron. **1**, 586 (2017), 1707.03021.
[16] S. L. Liebling and C. Palenzuela, Living Rev. Relativity **20**, 5 (2017), 1202.5809.
[17] P. O. Mazur and E. Mottola, Proc. Natl. Acad. Sci. U.S.A. **101**, 9545 (2004), gr-qc/0407075.
[18] C. Palenzuela, L. Lehner, and S. L. Liebling, Phys. Rev. D **77**, 044036 (2008), 0706.2435.
[19] M. Bezares, C. Palenzuela, and C. Bona, Phys. Rev. D **95**, 124005 (2017), 1705.01071.
[20] C. Palenzuela, P. Pani, M. Bezares, V. Cardoso, L. Lehner, and S. Liebling, Phys. Rev. D **96**, 104058 (2017), 1710.09432.
[21] T. Helfer, E. A. Lim, M. A. G. Garcia, and M. A. Amin (2018), 1802.06733.
[22] N. Sennett, T. Hinderer, J. Steinhoff, A. Buonanno, and S. Ossokine, Phys. Rev. D **96**, 024002 (2017), 1704.08651.
[23] M. Wade, J. D. E. Creighton, E. Ochsner, and A. B. Nielsen, Phys. Rev. D **88**, 083002 (2013), 1306.3901.
[24] R. A. Porto, Fortsch. Phys. **64**, 723 (2016), 1606.08895.
[25] N. V. Krishnendu, K. G. Arun, and C. K. Mishra, Phys. Rev. Lett. **119**, 091101 (2017), 1701.06318.
[26] A. Maselli, P. Pani, V. Cardoso, T. Abdelsalhin, L. Gualtieri, and V. Ferrari, Phys. Rev. Lett. **120**, 081101 (2018), 1703.10612.
[27] M. Vallisneri, Phys. Rev. D **77**, 042001 (2008), gr-qc/0703086.
[28] V. Cardoso, E. Franzin, A. Maselli, P. Pani, and G. Raposo, Boson star tidal deformability data, https://centra.tecnico.ulisboa.pt/network/grit/files/tidal-love-numbers/.
[29] P. Landry and E. Poisson, Phys. Rev. D **89**, 124011 (2014), 1404.6798.
[30] L. Wade, J. D. E. Creighton, E. Ochsner, B. D. Lackey, B. F. Farr, T. B. Littenberg, and V. Raymond, Phys. Rev. D **89**, 103012 (2014), 1402.5156.
[31] É. É. Flanagan and T. Hinderer, Phys. Rev. D **77**, 021502(R) (2008), 0709.1915.
[32] L. Blanchet, Living Rev. Relativity **17**, 2 (2014), 1310.1528.
[33] A. Buonanno, B. R. Iyer, E. Ochsner, Y. Pan, and B. S. Sathyaprakash, Phys. Rev. D **80**, 084043 (2009), 0907.0700.
[34] S. Khan, S. Husa, M. Hannam, F. Ohme, M. Pürrer, X. Jiménez Forteza, and A. Bohé, Phys. Rev. D **93**, 044007 (2016), 1508.07253.
[35] J. Vines, É. É. Flanagan, and T. Hinderer, Phys. Rev. D **83**, 084051 (2011), 1101.1673.
[36] K. Barkett et al., Phys. Rev. D **93**, 044064 (2016), 1509.05782.
[37] S. E. Gralla, Classical Quantum Gravity **35**, 085002 (2018), 1710.11096.
[38] T. Damour, A. Nagar, and L. Villain, Phys. Rev. D **85**, 123007 (2012), 1203.4352.
[39] T. Hinderer, B. D. Lackey, R. N. Lang, and J. S. Read, Phys. Rev. D **81**, 123016 (2010), 0911.3535.
[40] K. Yagi, Phys. Rev. D **89**, 043011 (2014), **96**, 129904(E) (2017), 1311.0872.
[41] J. Gagnon-Bischoff, S. R. Green, P. Landry, and N. Ortiz, Phys. Rev. D **97**, 064042 (2018), 1711.05694.
[42] K. Alvi, Phys. Rev. D **64**, 104020 (2001), gr-qc/0107080.
[43] T. Dietrich et al. (2018), 1804.02235.
[44] T. Damour and A. Nagar, Phys. Rev. D **81**, 084016 (2010), 0911.5041.
[45] T. Damour and A. Nagar, Phys. Rev. D **80**, 084035 (2009), 0906.0096.
[46] N. K. Johnson-McDaniel, N. Yunes, W. Tichy, and B. J. Owen, Phys. Rev. D **80**, 124039 (2009), 0907.0891.
[47] S. Bernuzzi, A. Nagar, M. Thierfelder, and B. Brügmann, Phys. Rev. D **86**, 044030 (2012), 1205.3403.
[48] D. Radice, L. Rezzolla, and F. Galeazzi, Mon. Not. R. Astron. Soc. Lett. **437**, L46 (2014), 1306.6052.
[49] T. Dietrich (private communication).
[50] B. P. Abbott et al. (LIGO Scientific Collaboration and Virgo Collaboration), Living Rev. Relativity **21**, 3 (2018), data available at https://dcc.ligo.org/LIGO-P1200087/public, 1304.0670.
[51] J. Veitch and A. Vecchio, Phys. Rev. D **81**, 062003 (2010), 0911.3820.
[52] J. Skilling, AIP Conf. Proc. **735**, 395 (2004).
[53] J. Veitch et al., Phys. Rev. D **91**, 042003 (2015), 1409.7215.
[54] A. Bohé et al., Phys. Rev. D **95**, 044028 (2017), 1611.03703.
[55] M. Colpi, S. L. Shapiro, and I. Wasserman, Phys. Rev. Lett. **57**, 2485 (1986).
[56] N. Sennett (private communication).
[57] I. Harry and T. Hinderer (2018), 1801.09972.
[58] P. Pani, L. Gualtieri, and V. Ferrari, Phys. Rev. D **92**, 124003 (2015), 1509.02171.
[59] P. Landry, Phys. Rev. D **95**, 124058 (2017), 1703.08168.
[60] T. Abdelsalhin, L. Gualtieri, and P. Pani (2018), 1805.01487.
[61] P. Landry (2018), 1805.01882.
[62] P. Pani, Phys. Rev. D **92**, 124030 (2015), **95** 049902(E) (2017), 1506.06050.
[63] N. Uchikata, S. Yoshida, and P. Pani, Phys. Rev. D **94**, 064015 (2016), 1607.03593.
[64] S.-M. Choi and H. M. Lee, Phys. Lett. **B758**, 47 (2016), 1601.03566.

SUPPLEMENTAL MATERIAL

Comparing boson star tidal deformability-mass relations with those of polytropic stars

In Fig. 2, we compare the tidal deformabilities (as a function of mass) for boson stars with a quartic self-interaction computed by [14] and available online at [28] with those of polytropic stars of different polytropic index. In order to make these curves comparable, we scale the masses by the maximum mass. We find that the tidal deformabilities for larger values of $\lambda_B =: \tilde{\lambda}_B (m_B/M_{\rm Pl})^2$ are well approximated by those of polytropic stars. We do not plot the results for the largest $\tilde{\lambda}_B$ or the solitonic

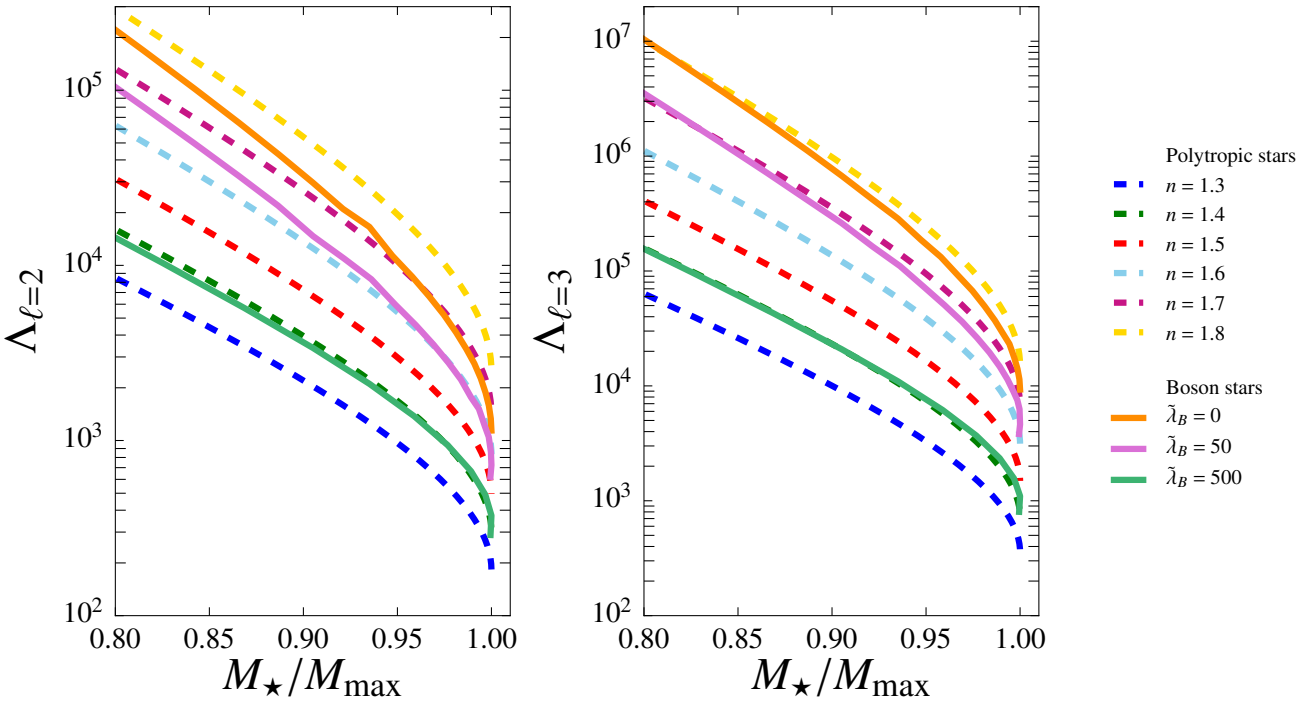

FIG. 2: The quadrupolar and octupolar tidal deformabilities for polytropic stars as well as those for boson stars with a quartic self-interaction computed by [14]. Both of these are plotted versus the star's mass $M_\star$, scaled by the maximum mass of a stable star with a given EOS, $M_{\rm max}$. Here n is the polytropic index and $\lambda_B =: \tilde{\lambda}_B (m_B/M_{\rm Pl})^2$, where m_B and λ_B are the boson mass and coupling constant and $M_{\rm Pl}$ is the Planck mass.

boson star model from [14, 28] as the data are not sufficiently finely sampled.

Checks of the contributions from higher-order terms in the phasing

We checked that various higher-order effects indeed lead to a small dephasing for the parameters we consider. In particular, we considered: i) the effects of the relative 1.5PN [i.e., absolute $O(v^{13})$] tidal tail term [Eqs. (B8)–(B10) and (B12) in Damour, Nagar, and Villain [38]]; ii) electric octupole tidal deformations [Eq. (91) in Yagi [40]]; iii) magnetic quadrupole tidal deformations [Eq. (6) in the erratum to Yagi [40] using the quasi-universal relation between the electric and magnetic quadrupole tidal deformabilities for irrotational stars from Eq. (31) and Table IX of [41] to give an order-of-magnitude estimate];[4] iv) the leading order correction due to linearizing in the quadrupole tidal deformability [Eq. (A5) in Hinderer *et al.* [39], with the corrections from the end of Appendix B in Yagi [40]]; and v) the effects of horizon absorption in a binary of nonspinning black holes [calculated starting from Eq. (11) in [42]]—this will be present in the waveform model, but the tidal heating effects for binaries of black hole mimickers are expected to be much smaller since their viscosities are expected to be much smaller than the effective viscosity of a black hole's horizon.

The dominant contribution is due to the 1.5PN tail term and the upper bound at the 90% credible level is < 1.5 rad for the cases we are considering. We do not use the 1.5PN phasing, since it does not agree as well with binary neutron star simulations as the 1PN phasing (see Fig. 10 in [43]), and the 2PN phasing is not known completely [38]. The dephasing from all the other contributions is at least an order of magnitude smaller, with the electric octupole tidal deformability giving the largest contribution, where the upper bound at the 90% credible level is < 0.11 rad. For comparison, the largest 90% bounds from the 0PN and 1PN tidal contributions are 6.1 and 2.7 rad, respectively.

[4] The fit from [41] gives the same order of magnitude and sign of the magnetic quadrupole tidal deformability found for boson stars in [14]. See Eqs. (6) and (20c) in [61] for the phase in terms of the magnetic quadrupole deformation quantity used in [41].

Calculation of the contact frequency

In this section, we use geometrized units with $G = c = 1$.

We compute the separation between the stars when their distorted surfaces come into contact, including the multipolar shape deformations through $\ell = 5$ and the first post-Newtonian (1PN) corrections to the quadrupolar and octupolar tidal fields, by solving

$$R_c = \left[1 + h_2^{(1)}\frac{m_2}{m_1}\left(1 - \frac{m_2}{2R_c} - \frac{M}{R_c}\right)\left(\frac{R_1}{R_c}\right)^3 + h_3^{(1)}\frac{m_2}{m_1}\left(1 - \frac{3m_2}{R_c} - \frac{M}{2R_c}\right)\left(\frac{R_1}{R_c}\right)^4 + h_4^{(1)}\frac{m_2}{m_1}\left(\frac{R_1}{R_c}\right)^5 + h_5^{(1)}\frac{m_2}{m_1}\left(\frac{R_1}{R_c}\right)^6\right]R_1 + (1 \leftrightarrow 2) \quad (1)$$

for the contact separation R_c, where m_A and R_A are the stars' masses and unperturbed radii, respectively, $M := m_1 + m_2$ is the binary's total mass, and $h_k^{(A)}$ is the kth shape (or surficial) Love number for star A [29, 45]. We compute each star's shape Love numbers and radius using its mass and the specific polytropic EOS we are considering. The expression for all ℓ to Newtonian order is $R_c = [1 + (m_2/m_1)\sum_{\ell=2}^{\infty} h_\ell^{(1)}(R_1/R_c)^{\ell+1}]R_1 + (1 \leftrightarrow 2)$, using the Newtonian potential of the star's companion at a distance of R_c to compute the electric tidal fields in Eq. (2.2) of [29] and taking the unit vector Ω_k in that paper's Eq. (2.6) to point towards the star's companion. The 1PN corrections to the quadrupole and octupole tidal fields come from Eqs. (B1a) and (B1c) in [46] evaluated at $t = 0$, noting that here we take $\Omega_k = -\hat{x}_k$ for the vector that points from star 1 to star 2 at $t = 0$. This generalizes the expression in Eq. (77) of Damour and Nagar [44] to include higher multipolar contributions to the tidal deformabilities and higher post-Newtonian corrections to tidal fields. The expression in square brackets in Eq. (1) is the fractional surface deformation of star 1.

We then solve this equation numerically for R_c, noting that there is a unique positive root for all contact radii for which we can possibly trust the post-Newtonian expressions used to obtain it. This follows because the shape Love numbers are all positive, so the right-hand side of the equation will be a decreasing function of R_c (for positive R_c) provided that the two terms from the 1PN corrections to the quadruple and octupole tidal fields are positive. Since the left-hand side is an increasing function of R_c (for positive R_c), there can thus only be one root. For the 1PN corrections to the quadruple and octupole tidal fields to be positive, it is sufficient to assume that $R_c > 3.5M$, and one would not want to consider much smaller separations using the post-Newtonian approximation.

We convert R_c to f_c, the binary's (dominant quadrupole mode) gravitational wave frequency at coalescence, using the 3PN point-particle relation, augmented with the tidal corrections. Specifically, we take the 3PN point particle relation between M/R_c and x_c [e.g., Eq. (231) in [32]] and expanding its reciprocal to 3PN. Here we take the gauge constant $r'_0 = M$ and use the Newtonian relation between x_c and M/R_c inside the logarithm. We use the expanded version of the reciprocal since this removes the η-independent terms at 2 and 3PN in the series. We then add on the quadrupole tidal pieces through 1PN from Eq. (2.9) in Vines, Flanagan, and Hinderer [35], and the higher-order tidal pieces through $\ell = 5$ to Newtonian order from Eq. (A6) in Yagi [40]. All of these contributions are linearized in the Love number. This gives

$$\begin{aligned}\frac{R_c}{M} = \frac{1}{x_c} - 1 + \frac{\eta}{3} + \left(\frac{19}{4} + \frac{\eta}{9}\right)\eta x_c + \left(-\frac{24257}{2520} + \frac{41}{192}\pi^2 - \frac{37}{12}\eta + \frac{2}{81}\eta^3 + \frac{22}{3}\log x_c\right)\eta x_c^2 \\ + \frac{2}{3}\left(\frac{m_2}{m_1}\left\{\left[3 - \left(3 - 13\frac{m_2}{M} + \frac{m_2^2}{2M^2}\right)x_c\right]\tilde{\lambda}_2^{(1)} + 4\tilde{\lambda}_3^{(1)}x_c^2 + 5\tilde{\lambda}_4^{(1)}x_c^4 + 6\tilde{\lambda}_5^{(1)}x_c^6\right\} + (1 \leftrightarrow 2)\right)x_c^4,\end{aligned} \quad (2)$$

where $x_c = (\pi M f_c)^{2/3}$ is the standard PN parameter (evaluated at the contact frequency), $\eta := m_1 m_2/M^2$ is the binary's symmetric mass ratio and $\tilde{\lambda}_\ell^{(A)} = k_\ell^{(A)}(R_A/M)^{2\ell+1}$ denotes a quantity related to the ℓth electric tidal Love number of the Ath star, scaled by $M^{2\ell+1}$ [cf. Eq. (9) in Yagi [40], but note that Yagi's $\bar{\lambda}_\ell$ is scaled using the individual star's mass, while we scale using the total mass of the binary, and do not include the usual numerical factors present in the definition of the Love number]. We solve this equation numerically. [Note that the leading-order tidal contribution inside the curly brackets is $\sum_{\ell=2}^{\infty}(\ell+1)\tilde{\lambda}_\ell^{(1)}x_c^{2\ell-4}$ to all orders.]

Note that we have not attempted to account for the difference in the Schwarzschild coordinate system used for the perturbed compact objects and the post-Newtonian harmonic coordinate system used for the binary. It is possible to estimate the effects of this coordinate transformation in the post-Newtonian approximation, using the binary black hole asymptotic matching results from [46] (though bearing in mind that the asymptotic matching calculation will be pushed to—and quite possibly beyond—the limits of its validity at the point of contact). Here, the leading-order effect is given by $r_{\rm PN} = r_{\rm Schw} - M_\star$, where $r_{\rm PN,\,Schw}$ denotes the radial coordinate in one of the two coordinate systems and $M_\star$ is the mass of the compact object the Schwarzschild coordinates are describing. (One would apply this transformation to the perturbed radii of the stars when computing the contact separation, which is given in PN harmonic coordinates.) This transformation thus increases the inferred contact frequency.

However, as in the initial calculation by Damour and Nagar [44], we do not use this transformation here: We found that the expression without the transformation reproduces the numerical relativity (NR) estimates of the contact frequency quite well, at least in the equal-mass $n = 1$ polytropic cases for which they are available. Specifically, Bernuzzi *et al.* [47] quote a dimensionless (dominant quadrupole mode) contact frequency of $Mf_c \simeq 0.078$ for a binary of equal-mass $n = 1$ polytropic stars with compactnesses of 0.16, while Radice *et al.* [48] report a dimensionless contact frequency of $Mf_c \simeq 0.11$ for a binary of stars with compactness 0.18. (Here M denotes the sum of the gravitational masses of the stars in isolation.) Our expression gives dimensionless contact frequencies Mf_c of 0.0778 and 0.111 for those two systems. (These values have estimated fractional errors

of $\lesssim 2\%$ each from the truncation of the PN expansion in the tidal fields or the radius-to-frequency conversion, and $\lesssim 1\%$ from the truncation in the multipole expansion of the tidal deformation. These errors are estimated using the ratio of the next-to-highest and highest order results.) While it is possible that the true values of these contact frequencies are higher, as this quantity is quite sensitive to the specific isodensity contour used to compute it, and generally increases with resolution [49], using the lower frequencies given by the expression without including the coordinate transformation is more conservative. In the future, we will compare our waveform model with numerical relativity waveforms (starting with those for binary neutron stars) to ascertain if our estimate of the contact frequency is an accurate guide for when the waveform model becomes inaccurate.

Bounds on the radii and fraction of maximum mass of the polytropic stars and cutoff frequencies used

We find that for the values of n for which we have sufficient numbers of samples with Λs above the minimum allowed by the EOS (i.e., just the ones to the left of the gap in the middle panel of Fig. 1, with n at most 0.9), we constrain the radii of the stars (at the 90% credible level) to be at most 2.6–3.5 times the Schwarzschild radius associated with their mass (increasing with increasing n); these range from 1.4 to 2.0 times the minimum radius allowed by the EOS. The masses of the stars are constrained to be within 0.6 to 0.9 of the maximum mass, with this fraction increasing with increasing n.

The upper cutoff frequencies used in our analysis range up to 1.2 times the dominant gravitational wave frequency corresponding to the innermost stable circular orbit of a Schwarzschild black hole with the same mass as the binary's total detector-frame mass, $f_{\rm ISCO} = [\pi 6^{3/2}(M_1^z + M_2^z)]^{-1}$ (in $G = c = 1$ units), in steps of 0.05. The lower cutoff frequency is always 15 Hz. The results shown come from upper cutoff frequencies of 0.8, 0.85, or 0.9 times $f_{\rm ISCO}$ for the cases to the left of the gap in Fig. 1, and $1.2 f_{\rm ISCO}$ for the ones to the right of the gap. The frequency of $1.2 f_{\rm ISCO}$ is still well below the binary black hole merger frequency (taken to be the frequency of the peak of the dominant mode of the waveform and computed using the fit from [54]) for all samples we consider. These upper cutoff frequencies correspond to orbital separations of $\sim$ 200–700 km for the systems considered.

Constraining parameters describing the polytropic EOS

For each simulated GW observation, we estimate the posterior distributions of the entire set of parameters (intrinsic and extrinsic) using the LALInferenceNest code, by truncating the likelihood integral at several different cutoff frequencies. Figure 3 shows the posterior distributions of the mass m_1 and tidal deformability Λ_1 of the more massive object (marginalized over all other parametrs), obtained from the simulated observation with $m_1^z = 39.5 M_\odot$ and $m_2^z = 31.7 M_\odot$. We show the cutoff frequencies employed in the calculation of these posteriors in the legend. The legend also shows the mean SNR $\bar{\rho}$ of the posterior samples — note that larger cutoff frequencies produce larger SNRs and hence narrower posteriors.

We compute the contact frequency assuming that both stars have the same polytropic index n, but possibly different polytropic constants K. Figure 3 assumes $n = 0.9$. The fraction of posterior samples with contact frequency (with $n = 0.9$) larger than the cutoff frequency employed is also shown in the legend. We then choose the largest cutoff frequency such that this fraction is larger than 0.9 (i.e., $f_{\rm cut} = 49$ Hz in Fig. 3) and read off the 90% credible upper limit on Λ_1 and the 90% credible lower limit on m_1. If the upper limit $\Lambda_{\rm UL}$ on the tidal deformability is smaller than the $\Lambda_{\rm min}$ corresponding to this EOS, the data exclude the possibility of both stars being described by this EOS at high confidence. Moreover, for a given polytropic index n, the lower limit $m_{\rm LL}$ on the component masses puts a lower limit on K, as described in the main text.

Constraints on boson mass and coupling constant

While binaries of boson stars with a quartic self-interaction are ruled out as sources of the injected signals at the 90% credible level, at higher credible levels, the upper bound on the tidal deformability is larger, and one only rules out some of the (m_B, λ_B) parameter space with the simulated observations. We thus consider the 95% credible level here, to illustrate these constraints on the parameter space, where we find that the least massive case can be produced by a binary of boson stars with a quartic self-interaction. (Note that > 95% of the samples have contact frequencies above the cutoff for the case we consider.)

The maximum mass and minimum tidal deformability of a stable boson star are given by [56]

$$M_{\rm max} \simeq 0.62\, w^{-1/2}\, \frac{M_{\rm Pl}^2}{m_B}, \tag{3a}$$

$$\ln \Lambda_{\rm min} \simeq 1.706 w^2 - 1.198 w^{3/2} + 0.828 w - 0.085 w^{1/2} + 5.66, \tag{3b}$$

where $M_{\rm Pl}$ is the Planck mass and $w := (1 + M_{\rm Pl}^2 \lambda_B / 64\pi m_B^2)^{-1}$. These approximate expressions (with fractional accuracies of a few percent) are obtained from fits to the computations in [22].

In Fig. 4, we show the constraints on m_B and λ_B from the 95% lower limit on the mass of the primary and 95% upper limit on the tidal deformability for the 15.5, 8.2 $M_\odot$ (detector frame) injection. For comparison, we also show the range of (m_B, λ_B) values that corresponds to a self-interaction cross-section per unit mass of $\sigma_B/m_B = 0.1$–1 cm^2/g. As discussed in [11], this range of

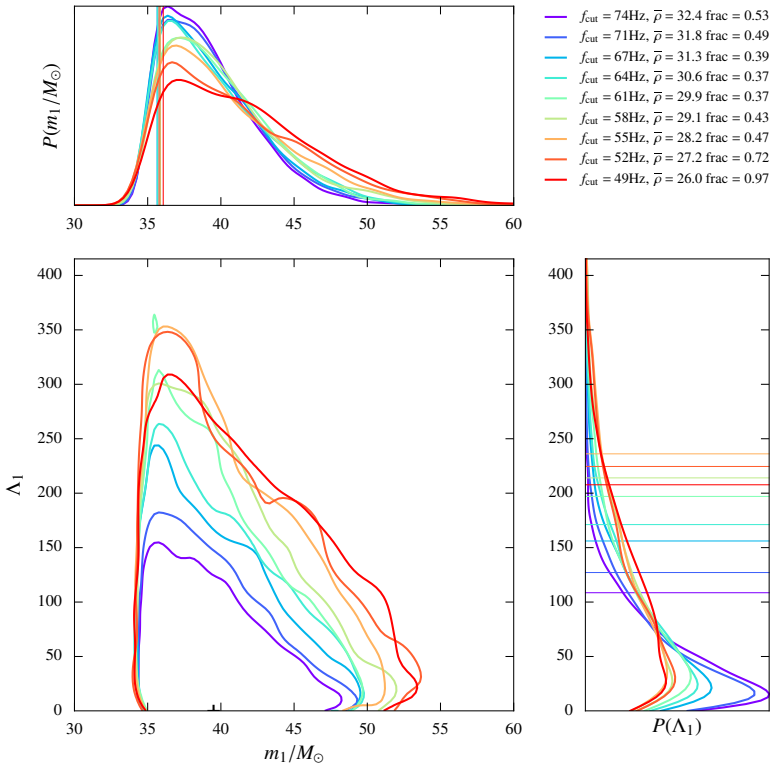

FIG. 3: Posterior distributions of the mass m_1 and tidal deformability Λ_1 of the more massive object (marginalized over all other parametrs), obtained from the simulated observation with $m_1^z = 39.5M_\odot$ and $m_2^z = 31.7M_\odot$. The middle panel shows the 90% credible regions in the marginalized posterior distribution $P(m_1, \Lambda_1)$ while top/side panels show the marginalized one-dimensional posteriors $P(m_1)$ and $P(\Lambda_1)$. The distributions are computed from the posterior samples using Gaussian kernel density estimates. The legends show the cutoff frequencies employed in the calculation of these posteriors, the mean SNR of the posterior samples and the fraction of posterior samples with contact frequency (computed using $n = 0.9$) larger than the cutoff frequency employed. The vertical lines on the top panel show the 90% credible lower bounds on m_1 while the horizontal lines on the side panel show the 90% credible upper bounds on Λ_1.

self-interaction cross-sections is the order of magnitude required for dark matter to explain various observations. For the purposes of this illustration, we assume that the Lagrangian used to describe the boson stars describes all the interactions of the complex scalar field and use the tree level cross-section $\sigma_B = (3/32\pi)(\lambda_B/m_B)^2$ calculated in [64]. The tree level approximation is very good everywhere except for the very highest boson masses we plot.

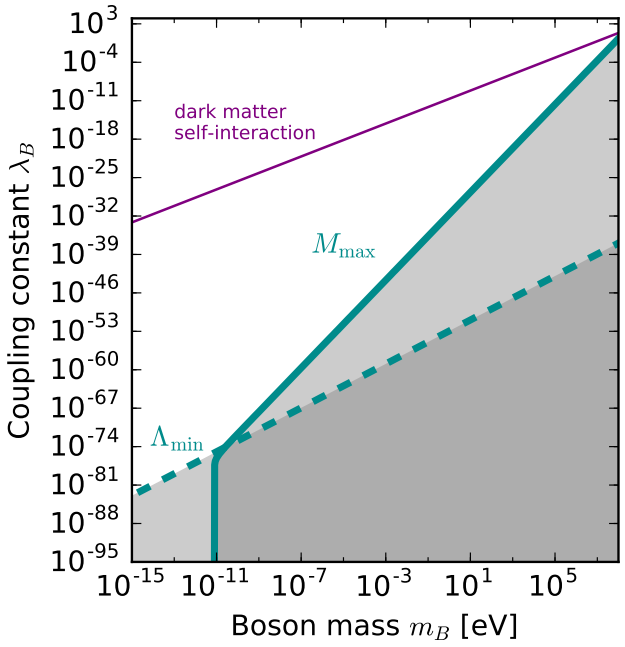

FIG. 4: Constraints on the parameter space of a boson star with quartic self-interaction from the $15.5, 8.2\ M_\odot$ (detector frame) injection using the fits in Eqs. (3) applied to the $n \geq 1.4$ results. Here m_B is the boson mass and λ_B is the coupling strength. The solid and dashed cyan curves correspond to the observed lower limit of $m_1 \geq 10.5 M_\odot$ and upper limit of $\Lambda \leq 298$ (both at the 95% credible level), respectively. The gray region is excluded at the 95% credible level. The purple line shows the parameters corresponding to a self-interaction cross-section per unit mass of 0.1–1 cm^2/g, as suggested for dark matter by various astronomical observations (discussed in, e.g., [11]).